

One- and three-dimensional quantum phase transitions and anisotropy in $\text{Rb}_2\text{Cu}_2\text{Mo}_3\text{O}_{12}$

S. Hayashida,^{1,*} D. Blosser,¹ K. Yu. Povarov,¹ Z. Yan,¹ S. Gvasaliya,¹
A. N. Ponomaryov,² S. A. Zvyagin,² and A. Zheludev^{1,†}

¹Laboratory for Solid State Physics, ETH Zürich, 8093 Zürich, Switzerland

²Dresden High Magnetic Field Laboratory (HLD-EMFL),
Helmholtz-Zentrum Dresden-Rossendorf, 01328 Dresden, Germany

(Dated: October 17, 2019)

Single crystal samples of the frustrated quasi one-dimensional quantum magnet $\text{Rb}_2\text{Cu}_2\text{Mo}_3\text{O}_{12}$ are investigated by magnetic, thermodynamic, and electron spin resonance (ESR) measurements. Quantum phase transitions between the gapped, magnetically ordered and fully saturated phases are observed. Surprisingly, the former has a distinctive three-dimensional character, while the latter is dominated by one-dimensional quantum spin fluctuations. The entire H - T phase diagram is mapped out and found to be substantially anisotropic. In particular, the lower critical fields differ by over 50% depending on the direction of applied field, while the upper ones are almost isotropic, as is the magnetization above saturation. The ESR spectra are strongly dependent on field orientation and point to a helical structure with a rigidly defined spin rotation plane.

I. INTRODUCTION

Frustrated $S = 1/2$ spin chains with competing nearest-neighbor J_1 and next-nearest-neighbor J_2 interactions are known to realize a panoply of exotic quantum phase such as chiral spin liquids [1–8], spin nematics [1, 4, 9–11] and spin density waves [4, 11, 12]. One of the most intriguing species of current interest is the linear chain molybdate $\text{Rb}_2\text{Cu}_2\text{Mo}_3\text{O}_{12}$ [13–15]. It is believed to feature a competition of ferromagnetic $J_1 = -138$ K and antiferromagnetic $J_2 = 51$ K ($|J_2|/|J_1| = 0.37$) interactions [14, 15]. The ground state is a spin singlet with a gap $\Delta \sim 1.6$ K in the excitation spectrum [16]. Powder samples have been extensively investigated by magnetic and dielectric measurements [17–19], high pressure studies [20, 21], NMR [22, 23], neutron scattering [19, 24] and muon spin relaxation measurements [19, 25]. The most interesting property is ferroelectric behavior that appears below 8 K despite the absence of any conventional magnetic order [17–19]. It was attributed to emergence of spin-chirality and the so-called spin-current or inverse Dzyaloshinskii-Moriya mechanism [26–29].

Unfortunately, a lack of single crystal samples severely hampers any further experimental progress. For instance, almost nothing is known about the magnetic phase diagram [23] or magnetic anisotropy in the system. In a breakthrough, we hereby present comprehensive magnetothermodynamic and electron spin resonance (ESR) measurements on $\text{Rb}_2\text{Cu}_2\text{Mo}_3\text{O}_{12}$ *single crystals*. We map out the entire H - T phase diagram down to 0.1 K in temperature and up to full saturation in magnetic field and find it to be highly anisotropic. The most intriguing result is that while the field-induced ordering transition is of a distinct three-dimensional character, the quantum

phase transition at saturation is entirely dominated by one-dimensional fluctuations.

II. EXPERIMENTAL DETAILS

Single crystal samples of $\text{Rb}_2\text{Cu}_2\text{Mo}_3\text{O}_{12}$ with typical mass 0.1 mg were grown by a spontaneous crystallization in a flux method [13]. Green transparent crystals were obtained as shown in Fig. 1(a). The crystal structure [monoclinic $C2/c$, $a = 27.698(7)$ Å, $b = 5.1010(15)$ Å, $c = 19.291(3)$ Å, $\alpha = 90^\circ$, $\beta = 107.31(3)^\circ$, $\gamma = 90^\circ$] was validated using single-crystal x-ray diffraction on a Bruker APEX-II instrument. It was found to be totally consistent with the previous report [13]. The magnetic properties are due to $S = 1/2$ Cu^{2+} cations. As illustrated in Figs. 1(b) and 1(c), CuO_4 plaquettes form one-dimensional (1D) chains along the crystallographic b axis. The individual chains are paired via MoO_4 bridges. The resulting chain-pairs are separated from one another by the Rb^+ ions.

Bulk measurements were carried out using the ^3He - ^4He dilution refrigerator insert for the Quantum Design physical property measurement system (PPMS). Heat capacity data were collected on a standard Quantum Design relaxation calorimetry option. The magnetic field was applied either along the crystallographic $a^* - c^*$ (transverse) or b (longitudinal) directions, correspondingly. Heat capacity was measured in the range of $0.1 \text{ K} \leq T \leq 1.7 \text{ K}$ and $0 \text{ T} \leq H \leq 14 \text{ T}$ without background subtraction. Magnetization measurements were carried out on a home-made Faraday force magnetometer. Field scans were collected at 0.1 K and 3 K up to 14 T, with the magnetic field along the $a^* - c^*$, $a + c$ and b axes, respectively. The absolute value of magnetization was obtained in a calibration measurement at 3 K using the vibrating sample magnetometer (VSM) for the PPMS. ESR measurements were performed using a 16 T transmission-type

* shoheih@phys.ethz.ch

† zhelud@ethz.ch; <http://www.neutron.ethz.ch/>

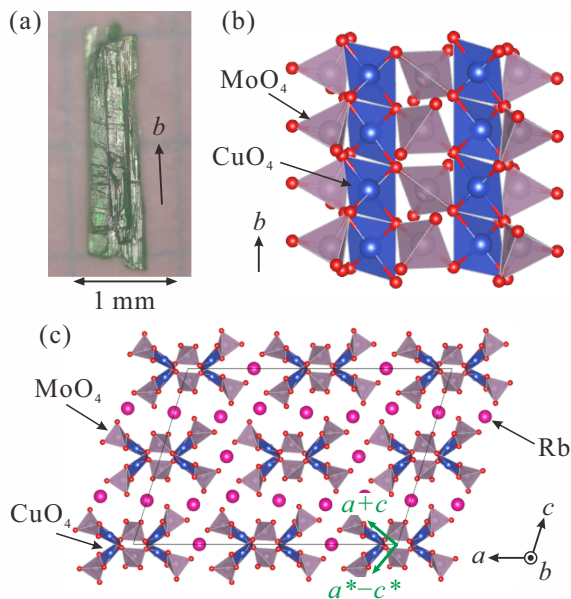


FIG. 1. (a) Typical single crystal $\text{Rb}_2\text{Cu}_2\text{Mo}_3\text{O}_{12}$ sample used in this work. (b),(c) Schematic view of the crystal structures of $\text{Rb}_2\text{Cu}_2\text{Mo}_3\text{O}_{12}$ (monoclinic, space-group $C2/c$).

ESR spectrometer, similar to that described in Ref. [30]. We measured field scans at 1.4 K at several frequencies. The experiments were set in the Faraday or Voigt configurations with the magnetic field applied along the $a^* - c^*$ and b axes, respectively.

III. RESULTS AND DISCUSSION

A. Heat capacity

Typical measured field dependencies of heat capacity are shown in Fig. 2. For the transverse and longitudinal field geometries, pairs of sharp lambda-anomalies are observed below 1.2 K and 0.9 K, correspondingly. We attribute these to a phase transition from the paramagnetic state to three-dimensional (3D) long-range order (LRO). In the low temperature limit the lower anomaly corresponds to a closure of the spin gap and the upper one to saturation. At higher temperatures the anomalies come closer together tracing a typical "dome" shape on the phase diagram [31]. For the two orientations studied, the critical fields at 0.1 K are $H_{c1,\perp} = 1.9$ T, $H_{c2,\perp} = 12.0$ T, $H_{c1,\parallel} = 3.0$ T, and $H_{c2,\parallel} = 11.4$ T for the transverse and longitudinal orientations, respectively. Strikingly, the upper critical fields are almost the same in the two geometries, but the lower ones differ by over 50%.

In addition to the sharp peaks, the field scans of specific heat show broad but prominent double-hump features (arrows in Fig. 2), particularly near saturation. Such features are typical of $d = 1$, $z = 2$ quantum criti-

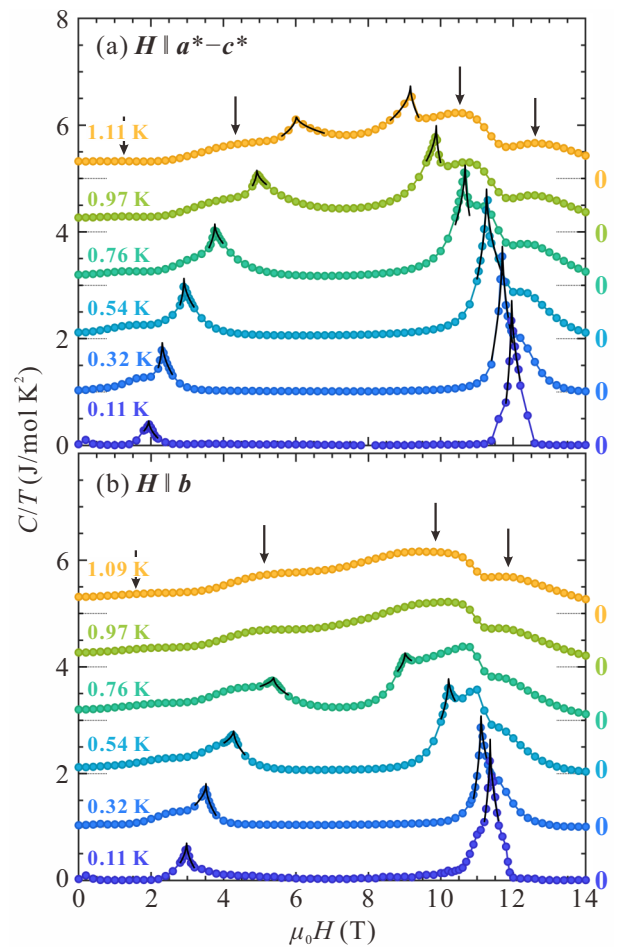


FIG. 2. Typical measured constant-temperature field scans of heat capacity in $\text{Rb}_2\text{Cu}_2\text{Mo}_3\text{O}_{12}$ for the transverse (a) and longitudinal (b) field geometries. Additional solid curves in the vicinity of sharp peaks are empirical power-law fits used to pinpoint the transition fields. Arrows indicate positions of additional broad features in the data, as described in the text. For visibility the scans are offset by 0.1 J/mol K^2 relative to one another.

cality [32, 33] and are also observed in other 1D materials magnets [34–36].

The temperature dependence of the heat capacity at zero field is shown in Fig. 3(a). Note the logarithmic scales on both axes. In full agreement with a gapped excitation spectrum, the low temperature behavior is exponentially activated. Assuming that a gapped quadratic one-dimensional dispersion relation for the low-lying excitations, the specific heat is given by $C_V \propto T^{3/2} \exp(-\Delta/k_B T)$ in the low-temperature limit $k_B T \ll \Delta$ [37, 38]. The activation temperature Δ/k_B is determined to be $1.9(1)$ K, which is roughly consistent with the lower critical field values.

In applied fields, across the domes of the 3D ordered phase, constant- H temperature scans of specific heat show distinct lambda anomalies at the phase boundary [Fig. 3(b)]. Most telling is temperature scans at precisely

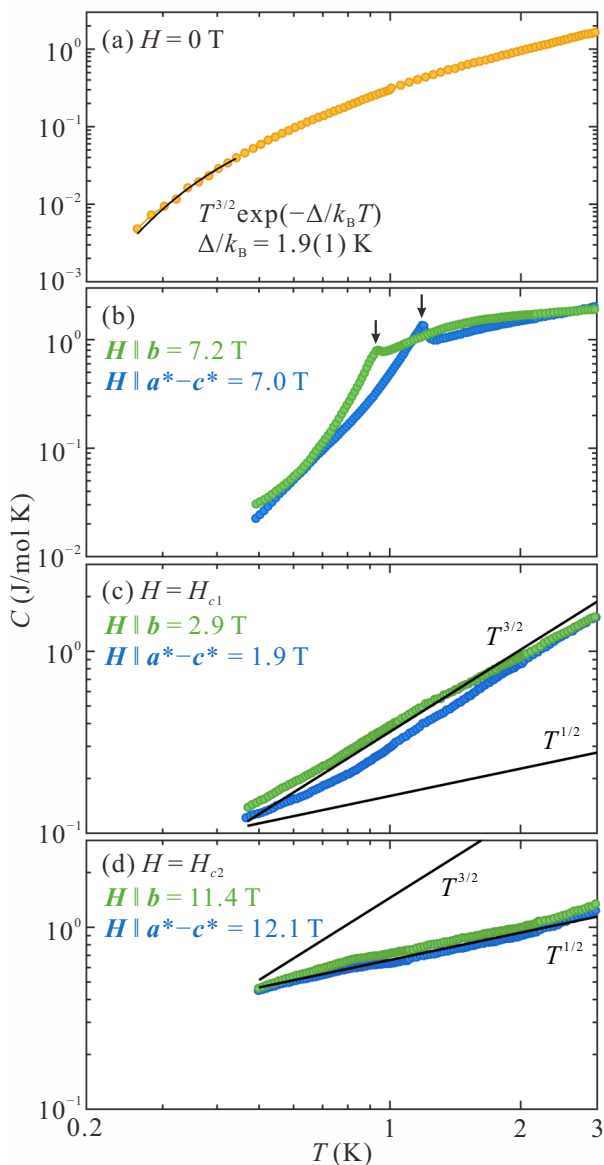


FIG. 3. Symbols: temperature scans of the heat capacity measured in $\text{Rb}_2\text{Cu}_2\text{Mo}_3\text{O}_{12}$ at different fields. (a) Zero applied field. The solid line is a fit of an exponentially activated form, as described in the text. (b) Intermediate fields. Arrows indicate lambda anomalies that represent long range magnetic ordering. (c),(d) Magnetic fields H_{c1} and H_{c2} corresponding to quantum phase transitions at gap closure and full saturation, respectively. The solid lines are power laws with exponents of $3/2$ and $1/2$.

H_{c1} and H_{c2} shown in Figs. 3(c) and 3(d) respectively. They reveal that, regardless of field geometry, the nature of the corresponding quantum critical points is markedly different. In general, for field-induced quantum phase transitions in gapped spin systems where magnons have a quadratic dispersion, we expect $C_V \propto T^{d/2}$ [39]. In this context, the lower transition behaves much as we would expect for 3D ordering, with $C_V \propto T^{3/2}$. In contrast, the criticality at H_{c2} must be dominated by one-dimensional

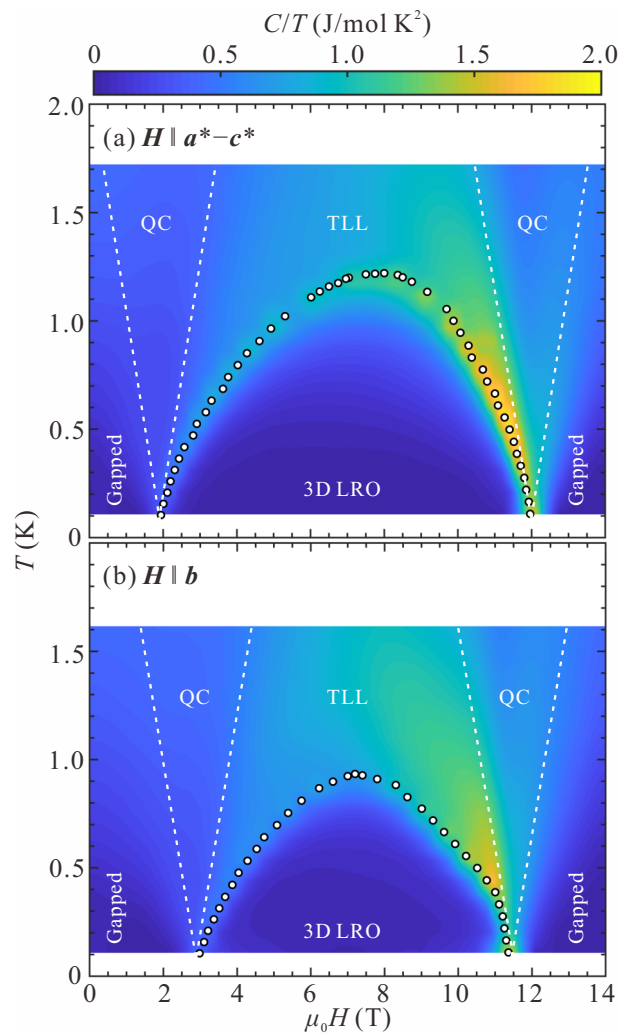


FIG. 4. Symbols: magnetic phase diagrams of $\text{Rb}_2\text{Cu}_2\text{Mo}_3\text{O}_{12}$ in the transverse (a) and longitudinal (b) geometries. The backgrounds show corresponding false color maps of $C(T, H)/T$. The phase regions are labeled as follows: three-dimensional long-range order (3D LRO), gapped, Tomonaga-Luttinger spin liquid (TLL), and quantum critical regime (QC). Dashed lines are guides for the eye.

fluctuations, as clearly $C_V \propto T^{1/2}$ provides a much better description of the data.

The bulk of the measured specific heat data was used to reconstruct the magnetic phase diagrams shown in Fig. 4 over false-color heat capacity plots. The symbols are boundaries of the 3D-ordered phase traced by the lambda anomalies in constant- T (Fig. 2) or constant- H [Fig. 3(b)] scans. The measured phase diagram is generally consistent with the one measured in powder samples with NMR [23]. The domes of the ordered phase are markedly anisotropic, with the maximal ordering temperature visibly suppressed in the longitudinal field configuration. For that geometry there is also a peculiar kink on the phase boundary at $H \sim 11$ T and $T \sim 0.5$ K. Also noteworthy is that the specific heats are strongly

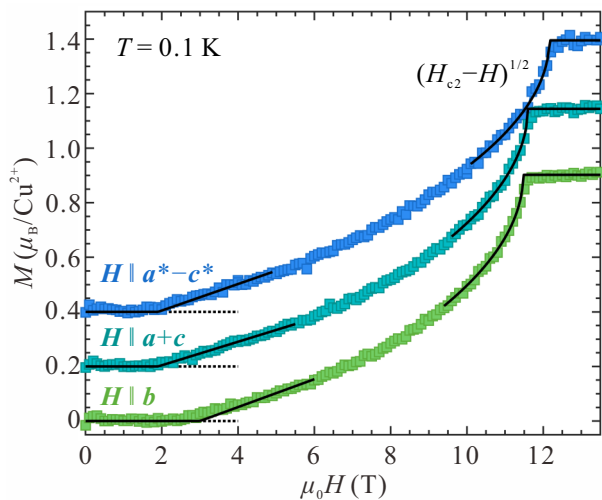


FIG. 5. Magnetization curves measured in $\text{Rb}_2\text{Cu}_2\text{Mo}_3\text{O}_{12}$ at $T = 0.1$ K in fields applied along three crystallographic directions (symbols). Solid lines are linear and square-root fits to the data in the vicinity of H_{c1} and H_{c2} , respectively. Two data sets are offset by $0.2 \mu_B$ and $0.4 \mu_B$ for visibility.

enhanced just above the upper boundary for both geometries.

B. Magnetization

Magnetization curves measured in $\text{Rb}_2\text{Cu}_2\text{Mo}_3\text{O}_{12}$ at $T = 0.1$ K for three field geometries are shown in Fig. 5. The nonmagnetic ground state below 2 T is confirmed. The transition fields at about 2 T and at about 11.5 T coincide with the critical fields H_{c1} and H_{c2} as measured with heat capacity. The saturated magnetizations are almost isotropic for the three orientations, and they are $0.99(1) \mu_B$ for $\mathbf{H} \parallel (\mathbf{a}^* - \mathbf{c}^*)$, $0.95(1) \mu_B$ for $\mathbf{H} \parallel (\mathbf{a} + \mathbf{c})$, and $0.90(1) \mu_B$ for $\mathbf{H} \parallel \mathbf{b}$. In all geometries the most striking feature is the different behaviors of magnetization in the vicinity of the critical fields. Near H_{c2} we see a distinct square-root approach to saturation. This is a hallmark of a $d = 1$ $z = 2$ quantum phase transition and is typical for one-dimensional Heisenberg spin systems [40]. In contrast, near H_{c1} , to within experimental noise, there is no sign of a square root singularity. Instead, we see a linear increase of magnetization. This mean-field behavior is typical of $d = 3$ $z = 2$ quantum criticality often referred to as a BEC of magnons [41, 42].

C. ESR

In low-temperature ESR experiments, in fields applied in either the longitudinal or transverse geometry, we observed a single resonance mode in all cases, as shown in the insets of Fig. 6. The main panel shows the measured field dependence of the resonance frequencies. In both

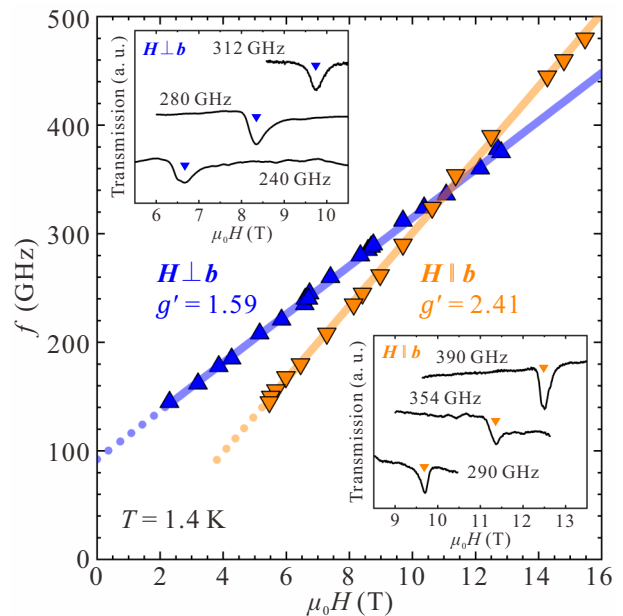


FIG. 6. Frequency-field diagram ESR excitations measured at $T = 1.4$ K. Solid lines are the fits of the linear function $\Delta + g'\mu_B H/h$. The insets show typical raw ESR spectra with characteristic transmission dips marking the resonance frequency.

geometries the behavior is linear in the accessible measurement range. Linear fits with $f = \Delta + g'\mu_B H/h$ yield $\Delta = 92.2$ GHz, $g' = 1.59$ for $\mathbf{H} \perp \mathbf{b}$ and $\Delta = -36.5$ GHz, $g' = 2.41$ for $\mathbf{H} \parallel \mathbf{b}$. The effective g' -factor is very different for the two geometries. They clearly do *not* correspond to the g factor of $\text{Rb}_2\text{Cu}_2\text{Mo}_3\text{O}_{12}$ which, based on the values of saturation magnetization discussed above, is very isotropic. One possible origin of this effect is that the ordered state is a spin spiral (helimagnet). In such systems the effective g' factor with applied field parallel to the spin rotation plane is known to be larger than in a transverse orientation. The ESR frequency dependence that we measure in $\text{Rb}_2\text{Cu}_2\text{Mo}_3\text{O}_{12}$ is indeed qualitatively similar to that seen in quasi-1D helimagnets such as LiCu_2O_2 [43], $\text{Li}_2\text{ZrCuO}_4$ [44], and LiCuVO_4 [45]. The key point, unlike in those materials, is that our ESR measurements at 1.4 K are above the ordering transition. This suggests that at 1.4 K one-dimensional spiral correlations are already well established in $\text{Rb}_2\text{Cu}_2\text{Mo}_3\text{O}_{12}$, or may even be a signature of three-dimensional chiral order in the system [2–4].

IV. CONCLUSION

Magnetic, thermodynamic and ESR measurements enabled by single crystal samples provide several important clues to the nature of quantum magnetism in $\text{Rb}_2\text{Cu}_2\text{Mo}_3\text{O}_{12}$: (i) There is a huge anisotropy of lower critical fields, while the upper critical fields and satura-

tion magnetizations are almost isotropic. (ii) At the lower critical field the quantum phase transition is a three-dimensional one with typical mean field behavior. The saturation transition, on the other hand, is dominated by one dimensional quantum fluctuations. (iii) Even at temperatures above the top of the LRO dome there is an indirect sign of strong helimagnetic spin correlations along the b axis. Magnetic anisotropy is thus a key ingredient in the rich physics of $\text{Rb}_2\text{Cu}_2\text{Mo}_3\text{O}_{12}$.

ACKNOWLEDGEMENTS

This work was supported by Swiss National Science Foundation under Division II, and Deutsche Forschungsgemeinschaft (DFG) through ZV 6/2-2 and SFB 1143. We acknowledge the support of the HLD at HZDR, member of the European Magnetic Field Laboratory (EMFL).

-
- [1] A. V. Chubukov, Phys. Rev. B **44**, 4693 (1991).
 [2] A. Kolezhuk and T. Vekua, Phys. Rev. B **72**, 094424 (2005).
 [3] T. Hikihara, L. Kecke, T. Momoi, and A. Furusaki, Phys. Rev. B **78**, 144404 (2008).
 [4] J. Sudan, A. Lüscher, and A. M. Läuchli, Phys. Rev. B **80**, 140402(R) (2009).
 [5] S. Furukawa, M. Sato, and S. Onoda, Phys. Rev. Lett. **105**, 257205 (2010).
 [6] S. Furukawa, M. Sato, S. Onoda, and A. Furusaki, Phys. Rev. B **86**, 094417 (2012).
 [7] H. Ueda and S. Onoda, Phys. Rev. B **89**, 024407 (2014).
 [8] H. Ueda and S. Onoda, Phys. Rev. B **90**, 214425 (2014).
 [9] L. Kecke, T. Momoi, and A. Furusaki, Phys. Rev. B **76**, 060407(R) (2007).
 [10] M. E. Zhitomirsky and H. Tsunetsugu, EPL (Europhysics Letters) **92**, 37001 (2010).
 [11] M. Sato, T. Hikihara, and T. Momoi, Phys. Rev. Lett. **110**, 077206 (2013).
 [12] S. Nishimoto, S.-L. Drechsler, R. Kuzian, J. Richter, and J. van den Brink, Phys. Rev. B **92**, 214415 (2015).
 [13] S. F. Solodovnikov and Z. A. Solodovnikova, J. Struct. Chem. **38**, 765 (1997).
 [14] M. Hase, H. Kuroe, K. Ozawa, O. Suzuki, H. Kitazawa, G. Kido, and T. Sekine, Phys. Rev. B **70**, 104426 (2004).
 [15] M. Hase, K. Ozawa, O. Suzuki, H. Kitazawa, G. Kido, H. Kuroe, and T. Sekine, J. Appl. Phys. **97**, 10B303 (2005).
 [16] Y. Yasui, R. Okazaki, I. Terasaki, M. Hase, M. Hagi-hala, T. Masuda, and T. Sakakibara, JPS Conf. Proc. **3**, 014014 (2014).
 [17] Y. Yasui, Y. Yanagisawa, R. Okazaki, and I. Terasaki, Phys. Rev. B **87**, 054411 (2013).
 [18] Y. Yasui, Y. Yanagisawa, R. Okazaki, I. Terasaki, Y. Yamaguchi, and T. Kimura, Journal of Applied Physics **113**, 17D910 (2013).
 [19] N. Reynolds, A. Mannig, H. Luetkens, C. Baines, T. Goko, R. Scheuermann, L. Keller, M. Bartkowiak, A. Fujimura, Y. Yasui, C. Niedermayer, and J. S. White, Phys. Rev. B **99**, 214443 (2019).
 [20] H. Kuroe, T. Hamasaki, T. Sekine, M. Hase, T. Naka, and N. Maeshima, AIP Conf. Proc. **850**, 1049 (2006).
 [21] T. Hamasaki, H. Kuroe, T. Sekine, T. Naka, M. Hase, N. Maeshima, Y. Saiga, and Y. Uwatoko, Journal of Magnetism and Magnetic Materials **310**, e394 (2007), proceedings of the 17th International Conference on Magnetism.
 [22] A. Yagi, K. Matsui, T. Goto, M. Hase, and T. Sasaki, J. Phys.: Conf. Ser. **828**, 012016 (2017).
 [23] K. Matsui, A. Yagi, Y. Hoshino, S. Atarashi, M. Hase, T. Sasaki, and T. Goto, Phys. Rev. B **96**, 220402(R) (2017).
 [24] K. Tomiyasu, M. Fujita, A. I. Kolesnikov, R. I. Bewley, M. Bull, and S. Bennington, Applied Physics Letters **94**, 092502 (2009).
 [25] S. Ohira-Kawamura, K. Tomiyasu, A. Koda, D. P. Sari, R. Asih, S. Yoon, I. Watanabe, and K. Nakajima, JPS Conf. Proc. **21**, 011007 (2018).
 [26] H. Katsura, N. Nagaosa, and A. V. Balatsky, Phys. Rev. Lett. **95**, 057205 (2005).
 [27] M. Mostovoy, Phys. Rev. Lett. **96**, 067601 (2006).
 [28] C. Jia, S. Onoda, N. Nagaosa, and J. H. Han, Phys. Rev. B **76**, 144424 (2007).
 [29] H. J. Xiang and M.-H. Whangbo, Phys. Rev. Lett. **99**, 257203 (2007).
 [30] S. Zvyagin, J. Krzystek, P. van Loosdrecht, G. Dhalenne, and A. Revcolevschi, Physica B: Condensed Matter **346-347**, 1 (2004).
 [31] V. Zapf, M. Jaime, and C. D. Batista, Rev. Mod. Phys. **86**, 563 (2014).
 [32] V. E. Korepin and N. A. Slavnov, Commun. Math. Phys. **129**, 103 (1990).
 [33] S. Sachdev, T. Senthil, and R. Shankar, Phys. Rev. B **50**, 258 (1994).
 [34] C. Rüegg, K. Kiefer, B. Thielemann, D. F. McMorrow, V. Zapf, B. Normand, M. B. Zvonarev, P. Bouillot, C. Kollath, T. Giamarchi, S. Capponi, D. Poilblanc, D. Biner, and K. W. Krämer, Phys. Rev. Lett. **101**, 247202 (2008).
 [35] O. Breunig, M. Garst, A. Klümper, J. Rohrkamp, M. M. Turnbull, and T. Lorenz, Science Advances **3**, eaao3773 (2017).
 [36] D. Blosser, V. K. Bhartiya, D. J. Voneshen, and A. Zheludev, Phys. Rev. Lett. **121**, 247201 (2018).
 [37] M. Troyer, H. Tsunetsugu, and D. Würtz, Phys. Rev. B **50**, 13515 (1994).
 [38] T. Hong, Y. H. Kim, C. Hotta, Y. Takano, G. Tremelling, M. M. Turnbull, C. P. Landee, H.-J. Kang, N. B. Christensen, K. Lefmann, K. P. Schmidt, G. S. Uhrig, and C. Broholm, Phys. Rev. Lett. **105**, 137207 (2010).
 [39] M. Continentino, *Quantum scaling in many-body systems* (Cambridge University Press, Cambridge, 2017).
 [40] J. C. Bonner and M. E. Fisher, Phys. Rev. **135**, A640 (1964).
 [41] E. G. Batyev and L. S. Braginski, Sov. Phys. JETP **60**, 781 (1984).
 [42] T. Giamarchi and A. M. Tsvelik, Phys. Rev. B **59**, 11398 (1999).

- [43] L. E. Svistov, L. A. Prozorova, A. A. Bush, and K. E. Kamentsev, *J. Phys.: Conf. Ser.* **200**, 022062 (2010).
- [44] T. Fujita, M. Hagiwara, M. Inada, Y. Yasui, and I. Terasaki, *JPS Conf. Proc.* **3**, 014028 (2014).
- [45] L. A. Prozorova, L. E. Svistov, A. M. Vasiliev, and A. Prokofiev, *Phys. Rev. B* **94**, 224402 (2016).